Journal of The Electrochemical Society, **153** (3) A472-A477 (2006)
0013-4651/2006/153(3)/A472/6/$20.00 © The Electrochemical Society

Micrometer-Scale Amorphous Si Thin-Film Electrodes Fabricated by Electron-Beam Deposition for Li-Ion Batteries

Jingtian Yin,[a] Masashi Wada,[b] Koichi Yamamoto,[b] Yasuyuki Kitano,[a] Shigeo Tanase,[a,*] and Tetsuo Sakai[a,*,z]

[a]*National Institute of Advanced Industrial Science and Technology (AIST), Kansai, Ikeda, Osaka 563-8577, Japan*
[b]*Fukuda Metal Foil and Powder Company, Limited, Nishinoyama, Yamashina-ku, Kyoto 607, Japan*

A series of micrometer-scale Si thin films were fabricated by electron-beam deposition on the Cu substrate with specially treated concave-convex surface. The combined analyses involving scanning and transmission electron microscopy, selected area electron diffraction, and X-ray diffraction revealed that the deposited Si layer possessed good adhesion to the substrate and a discontinuous amorphous microstructure in which there existed large amounts of interface regions. The surface changes of the Si thin-film electrodes during Li insertion and extraction were investigated by glow discharge optical emission spectroscopy. The half-cell tests showed that these thicker films had higher capacity and more impressive cycleability relative to those reported in the literature; their cycleability could be substantially improved by limiting Li insertion depth. The full-cell tests indicated that Si films thicker than 4 μm could provide sufficient capacity to match the standard $LiCoO_2$ cathode with a ~70-μm-thick coating layer. Such cells demonstrated small self-discharge rate as well as good cycling stability and efficiency in the long run, suggesting feasibility for potential practical applications.
 [DOI: 10.1149/1.2160429]

Manuscript submitted June 24, 2005; revised manuscript received November 9, 2005. Available electronically January 24, 2006.

Increasing attention has been devoted to developing high-energy-density anode materials for next-generation rechargeable lithium-ion batteries. Metal- or alloy-type anode materials possess much higher specific capacity and energy density than the currently used carbonaceous systems; therefore they are investigated extensively.[1-7] However, most alloy anodes reported to date showed serious capacity decay within several tens of cycles.

In our recent work, we have synthesized Ag–Sn, Ag–Sn–M (=Fe, Sb), and Ag–Sn–Fe/carbon nanotube systems with nanoscale heterophase structure by mechanical milling.[8-12] Some electrodes consisting of these alloys or composites could keep a rechargeable capacity of above 300 mAh/g over 300 cycles. Although these systems manifested superior cycle life, their large initial irreversible capacity loss (ICL) is still a problem to be solved for practical applications.

Silicon appears to be a promising candidate for the anode material due to its high theoretical specific capacity (~4200 mAh/g for $Li_{4.4}Si$), low electrochemical potential vs Li/Li^+ (between 0 and 0.4 V), and small initial ICL compared to other metal- or alloy-type anode materials.[13-27] However, some great issues strongly limit its practical applications. It has been reported that the bulk silicon with well-crystallized structure can hardly react with lithium to form highly lithiated Li_xSi (e.g., $x = 4.4$) at room temperature.[28-30] The uncompleted lithiation results in a low efficiency in specific capacity for the Si electrodes. Furthermore, this material undergoes dramatic volume changes (~300%) during lithiation and delithiation, resulting in disintegration of the electrodes and subsequent rapid capacity fading.

Recent investigations demonstrated that the amorphous Si thin-film electrodes fabricated by various deposition methods showed substantially improved electrochemical performance both in specific capacity and cycleability. Graetz and co-workers reported that the 100-nm-thick Si thin film prepared by physical deposition gave a specific capacity of around 1100 mAh/g with a 50% capacity retention after 50 cycles.[28,29] Maranchi et al. claimed that the 250-nm films deposited by radio-frequency (rf) magnetron sputtering exhibited reversible capacities of ~3500 mAh/g for 30 cycles.[30] Takamura and co-workers found that the 50- and 150-nm Si thin films vacuum-deposited onto a Ni foil could deliver capacities of ~3500 and ~2200 mAh/g, respectively, for 200 cycles.[31,32]

Despite the excellent performance, the above Si films still cannot be employed in the practical batteries because they are too thin to provide sufficient capacity for matching the commercialized cathode material. Thus, it is highly desired to obtain the Si films with several micrometers of thickness. However, numerous studies showed that increasing the thickness of Si thin films affected seriously their electrochemical behaviors. The results obtained by Maranchi et al. showed that reversible capacities of 3000 mAh/g could be maintained only within 12 cycles for 1-μm-thick Si film.[30] Bourderau et al. also reported that 1.2-μm-thick thin films gave a specific capacity of ~1000 mAh/g but a poor cycling ability after the first three cycles.[16] Therefore, the issue of how to expand the film thickness without sacrificing cyclability and specific capacity is becoming the focus of research at the present stage.

So far, the most impressive reports on the Si thin-film electrode should belong to Sanyo's group. Yoshida et al.[25] and Yonezu et al.[26] have reported that an amorphous film (5-μm-thick) deposited on a moderately roughened surface of copper foil by a plasma chemical vapor deposition (CVD) or an rf magnetron sputtering method delivered an initial discharge capacity of 3590 mAh/g and did not show obvious capacity decay in ten cycles. The excellent performance was attributed to the formation of microcolumns, which maintained good adherence with the copper foil during cycling. In addition, Takamura et al. have also reported that a 4.8-μm-thick Si film could maintain a capacity of ~1200 mAh/g for about 120 cycles.[33]

In this work we attempted to fabricate a series of Si thin films with different thickness by means of electron-beam deposition. The electrochemical behaviors of the Si films were investigated and discussed in relation with their microstructure and surface changes. Some thicker films were also coupled with commercialized $LiCoO_2$ cathodes to examine their electrochemical behaviors in practical batteries.

Experimental

Si thin films were deposited on LB3-type Cu foil (around 16 μm in thickness, Fukuda Metal Foil & Powder Co., Ltd.) by electron-beam deposition using high-purity Si wafer (99.99%) as a target. The depositing rate was predetermined by depositing the Si films on special smooth glass substrates and measuring the functional relationship between the thickness and deposition time. According to different deposition times, a series of Si thin films with various thicknesses were fabricated. The thickness of the Si thin films was verified by cross-sectional scanning electron microscopy (SEM) or

* Electrochemical Society Active Member.
z E-mail: sakai-tetsuo@aist.go.jp

Table I. The characteristics of the coating layer of $LiCoO_2$ cathode.

Composition (atom %)	Thickness (μm)	Density (g/cm^3)	Geometrie capacity (mAh/cm^2)
90% $LiCoO_2$ + 5% KB + 5% PVdF	70 ± 2	~2.2	~2.0

transmission electron microscopy (TEM) analysis. These thin-film electrodes were cut into circular sheets of 1.13 cm^2(∅12) in area and vacuum-dried at 120°C for 3 h prior to using.

Electrochemical studies were performed on 2032-type coin cells with: (i) lithium metal (0.5-mm-thick foil) and (ii) standard $LiCoO_2$ as counter electrodes. The properties of the cathode material are shown in Table I. The electrolyte used in this work was 1 M $LiPF_6$ in 1:1 EC/DEC(v/v). Cell assembly was performed in a dry room with a dew point of about -70°C. Half-cell tests were carried out between 0.00 and 1.00 V (vs Li) under a C/10 rate (based on theoretical capacity of silicon) at a constant temperature of 25°C. All cell tests were carried out between 4.2 and 3.0 V in different C rates.

Structural, morphological, and microstructural analyses for fabricated Si films were carried out with X-ray diffraction (XRD) with Cu Kα radiation, SEM, and TEM (300 kV H9000NA, Hitachi). The surface characterization of the electrodes during cycling was accomplished by glow discharge optical emission spectroscopy (GD-OES) with rf (JY-5000RF, Horiba, Japan). All the cells for the surface characterization were polarized to the required voltages using a small current density of 0.1 mA/cm^2. The samples for GD-OES analysis were prepared inside an argon-filled glove box.

Results and Discussion

Microstructure and morphology.— Figure 1 shows the surface and cross-sectional SEM images of LB3-type Cu foil substrate. It is evident that this type of Cu substrate has a rough surface that has been specially treated into a concavo-convex shape for the Si deposition. Figure 2 displays the surface and cross-sectional morphologies of the 6-μm Si thin film deposited on the above substrate. From SEM observation (Fig. 2a), it is known that the surface of the deposited film has also a rough morphology like its substrate. The TEM observation indicates that the thicker Si film shows a columnar structure in cross section, in which pillars are separated from one another by dense "grain" boundaries. No peeling off is observed, suggesting good adhesion of the Si layer on the Cu substrate.

The enlarged cross-sectional TEM image of the deposited film is shown in Fig. 3a. In the microstructure of the Si layer, bundle-shaped dendrites are clearly observed (upper right); the growth direction of the layer is approximately perpendicular to the bottom of the Cu substrate (lower left). The inset of Fig. 3a illustrates the selected-area electron diffraction (SAED) pattern taken from the Si layer. It is seen that the diffraction pattern consists of diffused haloes, different from clear rings/spots of crystalline Si phase. This suggests that the deposited film is formed by amorphous structure.

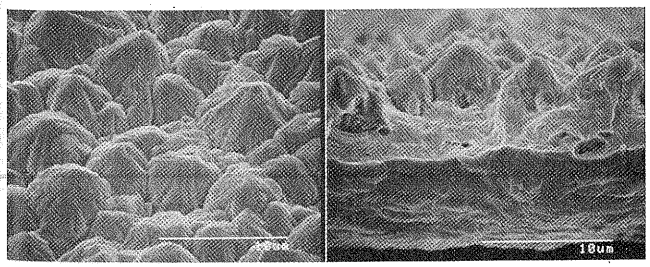

Figure 1. SEM images of LB3-type Cu substrate: surface (left) and cross-section (right).

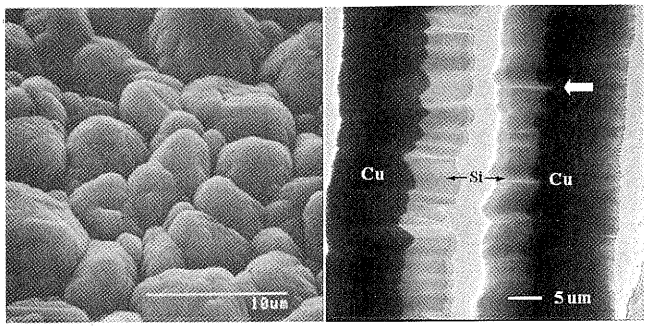

Figure 2. Morphologies of the 5 μm thick Si thin film deposited on Cu substrate: surface SEM image (left) and cross-sectional TEM image (right).

Figure 3b shows the structural discontinuity of the deposited film caused by the surface roughness. It is likely that the concave or convex substrate leads to more or less deviation of the growth direction of the Si layer. As a result, the interfaces or grain boundaries are formed during deposition at places where the growth of dendrites begins to obstruct one another. It is reasonably expected that the degree of discontinuity is much higher in the thicker film.

Figure 4 presents the XRD pattern of the Si film deposited on Cu substrate. Except for three strong diffraction peaks corresponding to the copper substrate, none of the Si peaks can be detected within

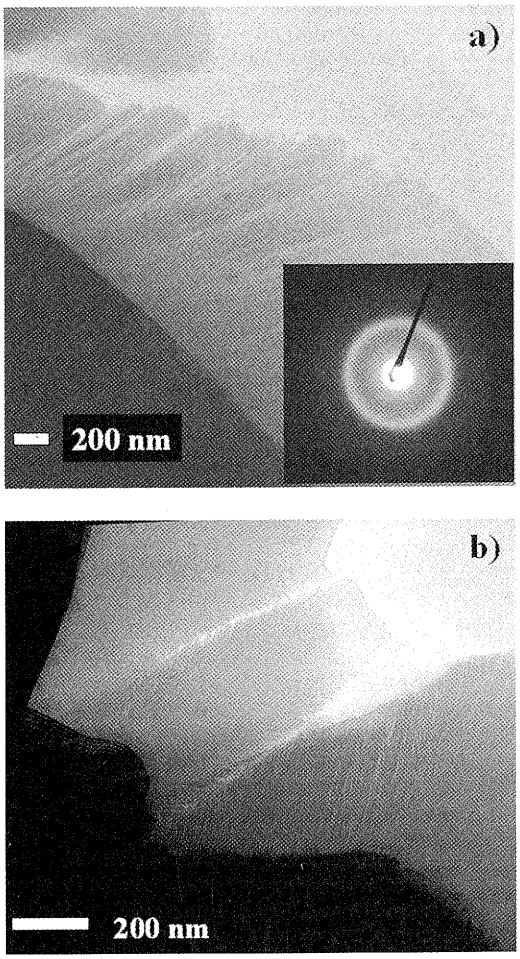

Figure 3. Cross-sectional TEM images (a and b) and corresponding SAED pattern (inset of Fig. 3a) of the Si thin film electrode.

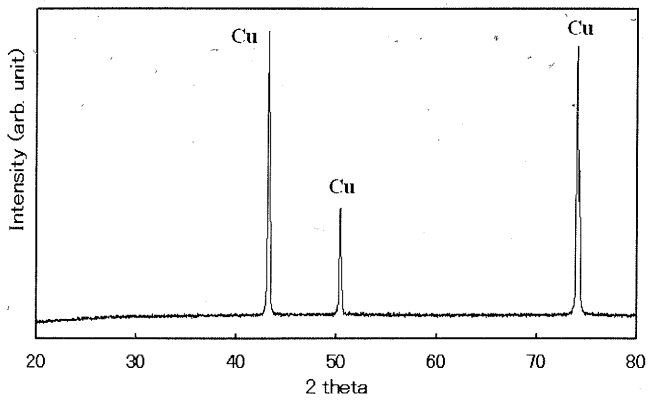

Figure 4. XRD pattern of the Si thin-film electrode deposited on Cu substrate.

measurable limits. This result also suggests that the Si thin film is formed by the amorphous structure, inconsistent with the electron diffraction result.

Electrochemical half-cell tests using metallic Li as counter electrode.— Figure 5a presents the voltage profiles of 0.2- and 2-μm Si film electrodes for the first cycle. Figure 5b compares the cycling performance of the Si film electrodes with different thicknesses. The use of gravimetric units for evaluating the capacity of such thin films with discontinuous structure could generate more or fewer errors. For accuracy and convenience, geometric units are used hereafter. Comparing these curves shows that the cycling performance is strongly influenced by the thickness of the Si layer, i.e., the thinner

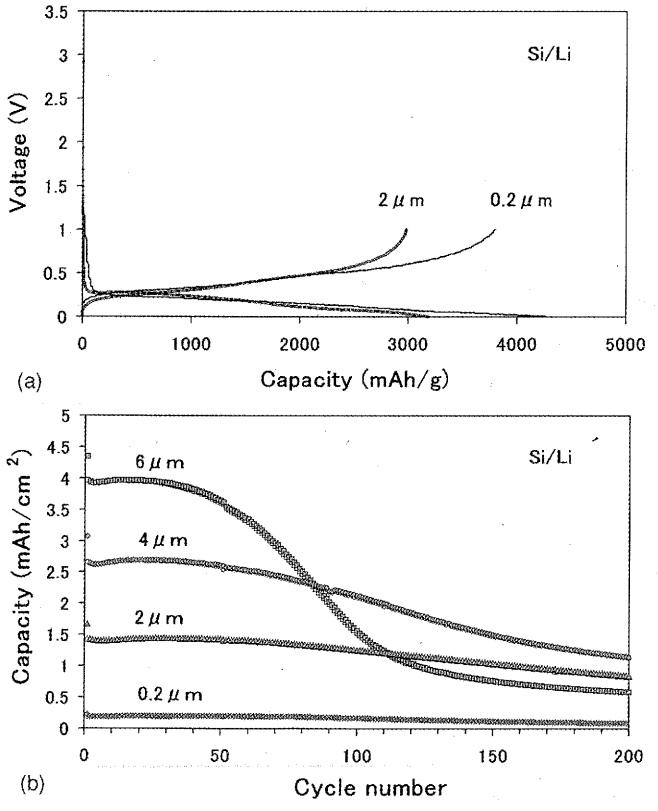

Figure 5. Voltage profiles of 0.2- and 2-μm Si film electrodes for the first cycle (a) and the cycling performance of the Si film electrodes with various thicknesses (b). Solid and open symbols represent Li insertion and extraction capacity, respectively.

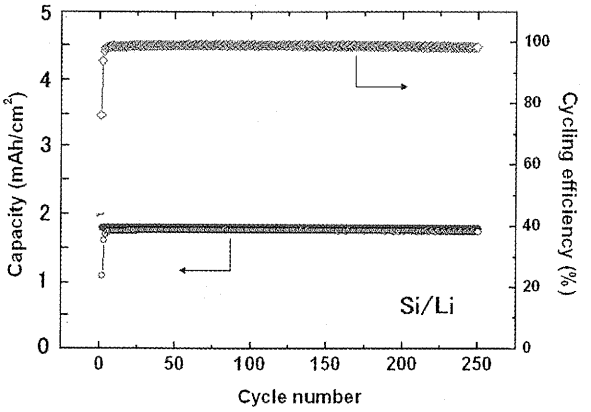

Figure 6. Cycling performance and efficiency of the 6-μm film electrode under the condition of limiting Li insertion depth at 1.8 mAh/cm^2 (around 45% of the reversible capacity of the 6-μm film electrode). Solid and open symbols represent charging and discharging capacity, respectively.

the deposited film, the better the capacity retention. The 0.2-μm film exhibits the best cycling stability, keeping a relative stable capacity of ~0.18 mAh/cm^2 (~3800 mAh/g) for a long-term run. The 2-μm film electrode delivers a reversible capacity of ~1.2 mAh/cm^2 (~3400 mAh/g), which does not undergo any capacity fading up to 50 cycles but gradually decreases to ~0.9 mAh/cm^2 after 200 cycles. The capacity loss rate is calculated to be 0.2% per cycle between 1 and 200 cycles. According to the recent reports of the Si thin-film electrodes, it is known that 1-μm-thick Si film could maintain a capacity of ~3000 mAh/g only within 12 cycles, and 1.2-μm-thick Si films gave a capacity of ~1000 mAh/g but a poor cycling ability after the first three cycles.[16,30] Compared with these electrodes, the 2-μm film electrode fabricated in this work exhibits significant improvement both in specific capacity and cycling stability. The thicker 4- and 6-μm films provide reversible capacities of 2.6 and 4 mAh/cm^2, respectively, both of which can be maintained for several tens of cycles. As reported by Sanyo's group,[25,26] the 5-μm-thick Si film exhibited a capacity greater than 3000 mAh/g and no capacity decay in ten cycles. Compared to the result, the 6-μm-thick Si film in this work shows a slightly lower capacity (~2900 mAh/g) but a longer cycle life.

Figure 6 shows the cycling performance and efficiency of the 6-μm film electrode under the condition of limiting Li insertion depth at 1.8 mAh/cm^2. In this case, one can see that the electrode shows superior cycling stability upon long-term cycling; the cycling efficiency rises up to ~97% in the third cycle and remains greater than 98% over 250 cycles. The generally accepted explanation is that when Li insertion is limited in a lower compositional range by controlling charging depth, the volume expansion of the Si electrode is suppressed and thus the cycling stability is improved.

Relationship between microstructure and cycling behaviors.— Figure 7 shows the surface and cross-sectional SEM images for the 6-μm film electrode after completion of the 250 cycles under the condition of limiting Li insertion depth at 1.8 mAh/cm^2. It is seen that the Si layer still keeps good adhesion to the Cu substrate in spite of severe vertical fraction. The morphology of the Si film after long-term cycling is quite similar to that (after first fully charging and discharging) reported by Sanyo's group. In their study, the Si film was extended from 5 to 17 μm after the first charge and was divided into microcolumns after the first discharge. However, each column was not peeled off from the copper current collector. They attributed the good adhesion to the following reasons: *(i)* expanded contact area by the roughened surface of Cu foil; *(ii)* formed intermixed layer of active mass and underlying material during a vacuum process, and *(iii)* a stress relaxation mechanism (i.e., concentration of

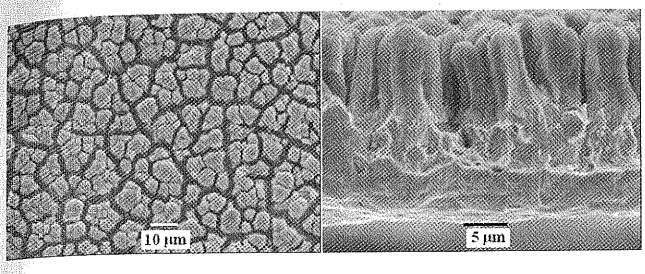

Figure 7. Surface (left) and cross-sectional (right) SEM images for the 6-μm film electrode after 250 cycles under the condition of limiting Li insertion depth at 1.8 mAh/cm^2.

the stress at the valley of irregularities but dispersed stress at the rest during the first charge–discharge).

In this work, the effects of the microstructure on the cycling behaviors can be argued as follows. First, amorphous structure would be an essential factor responsible for the improved electrochemical behaviors of these electrodes. Some studies have reported that amorphous Si structure is more open compared with well-crystallized one and might cause homogeneous volume expansion/contraction by eliminating the existence of any two-phase regions during cycling.[20,28,29] Second, the concavo-convex surface of the Cu substrate increases the adhesion of Si layer on the Cu substrates and the endurance of Si layer against repeated expansion and contraction during cycling. The third beneficial factor could be attributed to the structural discontinuity of the deposited film. The discontinuous structure results in the formation of large amounts of interface regions (see Fig. 3b). The interface regions could buffer to some extent the volume expansion upon Li insertion. The interface zones are also key places where cracks yield and propagate during cycling. The presence of these defects vertical to the substrate would prompt the vertical fracture of the Si layer upon repeated action of stresses and reduce the possibility of forming horizontal cracks, especially for thicker Si films.

Surface changes accompanying Li insertion and extraction.— Figure 8 presents the discharge and charge (corresponding to Li extraction and insertion, respectively) profiles of the 2-μm thin-film electrode for the first cycle. To clarify the surface changes of the Si thin-film electrodes during Li insertion and extraction, GD-OES analysis was performed at the certain given voltage points (corresponding to ①–④ points in Fig. 8). The results are shown in Fig. 9a–d. In Fig. 9a, the thickness of the silicon layer obtained by GD-OES seems to be less than its actual thickness of 2 μm. The depth profile by the GD-OES method is sensitive to the component elements. When nonmetallic elements with light atomic masses are that contained, the depth values would not be as accurate. In the present work, the thickness changes of the coating layer measured by GD-

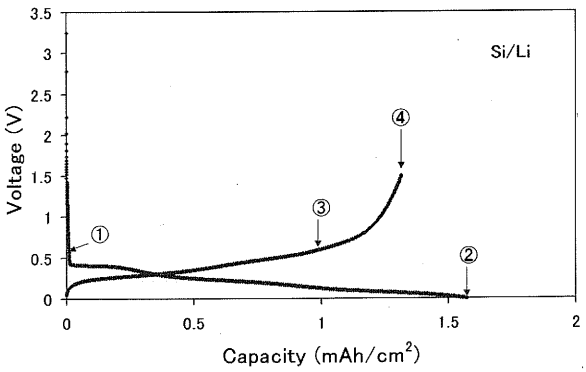

Figure 8. Voltage profiles of the 2-μm thin film electrode for the first cycle. Numbers of ①–④ represent the given voltage points.

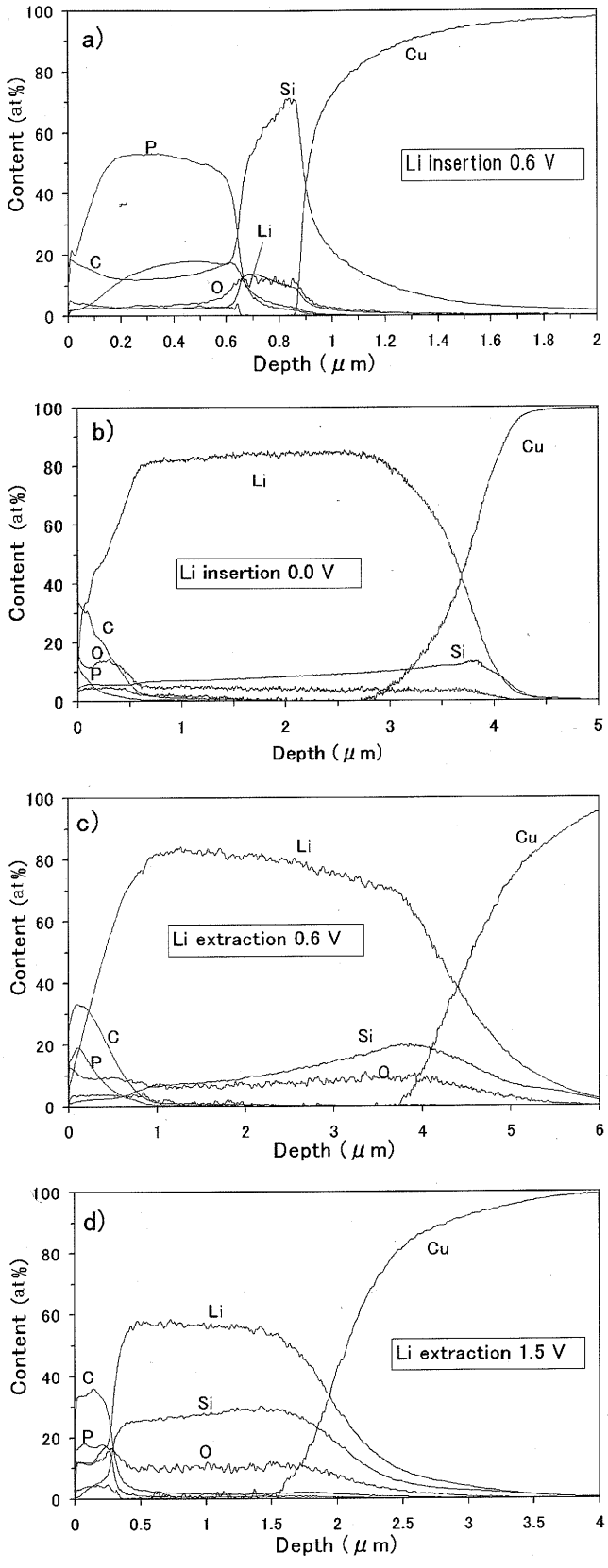

Figure 9. GD-OES depth profiles of the 2-μm Si film electrodes in four different Li insertion and extraction states.

OES show more qualitative rather than quantitative significance. When the solid electrolyte interphase (SEI) layer is almost removed, the measured depth of the Si layer became quite close to the real value, as shown in Fig. 9d.

At the beginning of Li insertion (0.6 V), in addition to element Si, the compositions observed on the outermost surface include P, C, O, Li, F, H, etc. Because the detectable signals of H and F are quite weak compared to others, their elemental distributions are neglected in the study for simplicity. The depth profile shows that rather low Si content could be detected in near-surface layer. This implied that the surface of the Si film was covered by the SEI layer, i.e., the decomposed products of electrolyte and remaining electrolyte. In the Si-rich inner layer, the contents of O and Li increase while the contents of P and C decrease. Apart from those oxide impurities formed in the processes of sputter deposition or preparing electrodes, the relatively high O content in the interior region could also be attributed to the oxidization of active material by contacted electrolyte. Because the reaction potential of Si with Li is lower than 0.6 V, the increased Li in the inner layer may be related to the reaction of oxygen with Li.

Upon Li insertion to 0.0 V, the near-surface region becomes thicker than that formed at 0.6 V, suggesting that the SEI layer formed on the surface of the thin-film electrodes swells with the expansion of the Si film. The Li content of the Si layer increases strongly accompanied by an approximately 3–4 times increase in thickness, reflecting the formation of highly lithiated Li_xSi. However, the content of oxygen does not increase with deep Li insertion. This indicates that the SEI layer prevents the active material from further contacting electrolytes and hence, few silicon oxides are yielded in this stage.

Upon Li extraction (shown in Fig. 9c–d), the Si content increases progressively with the decrease of Li content, indicating that Si phase starts to recover from its lithiated phases Li_xSi. This process is accompanied by shrinkage of the Si layer. However, considerable Li content remains in the Si layer, and the Si layer does not return completely to its original geometry even at 1.5 V, suggesting an incomplete recovery. It is also found that the outer SEI-layer shrinks with the Li extraction process but the content of oxygen increases in the interior region. The reason for this would be associated with the breakage of SEI layer due to the large volume changes of the electrodes. In the Li extraction process, the SEI layer suffers from severe shrinkage of the inner active material. As it is broken, the electrolyte would permeate through the damaged SEI layer and react with the inner active material to form silicon oxides. The mechanism is similar to that of AgSn film electrode, which has been described in detail in our previous work.[34] The above analysis shows that the unstable SEI layer and the residual lithiated phases are most likely the reason for the irreversible capacity loss.

Electrochemical full-cell tests using $LiCoO_2$ as cathode.— In this section, the Si thin-film electrodes were combined with standard $LiCoO_2$ cathodes into full cells to test the practical application for Li-ion rechargeable batteries. As shown in Table I, the standard $LiCoO_2$ cathode with a ~70-μm-thick coating layer has a geometric capacity of ~2.0 mAh/cm^2. In order to match this capacity, the thickness of Si thin films should not be less than 3 μm in terms of a rough calculation for the previous results (Fig. 5b). The previous results have also shown that limiting Li insertion depth could improve substantially the cycleability of thicker Si film electrodes. Based on these considerations, we selected 4- and 6-μm films (corresponding to reversible capacities of 2.6 and 4.0 mAh/cm^2, respectively) as anodes to match the standard $LiCoO_2$ cathodes.

Figure 10 shows the cycling performance of both full cells between 3.0 and 4.2 V. As can be seen, the electrochemical behaviors are almost the same for the two cells. The relatively large irreversible capacity loss (~20%) during the first cycle should be attributed to the electrolyte decomposition reactions through formation of the SEI layer on the Si film surface and the residual lithiated phases within the Si layer as explained by GD-OES. After the first cycle,

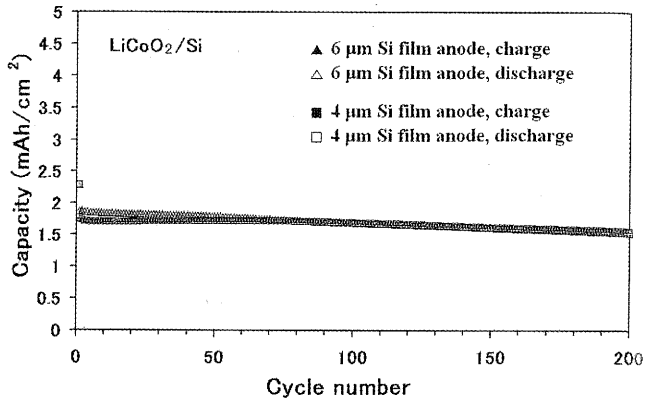

Figure 10. Cycling performance of full cells (using 4- and 6-μm thick Si films as an anode, respectively) between 3.0 and 4.2 V.

the charge and discharge capacity values overlap, suggesting quite good cycling efficiency (>99%). Both cells show superior cycling stability in the long run. The reason for this is most likely because the capacity of $LiCoO_2$ is far less than that of Si film anodes. Further work should be conducted to optimize the suitable capacity ratio of anode to cathode (A/C).

Figure 11 shows the rate capability of a cell using 4-μm-thick Si film as an anode. It is seen that the capacity decreases with the increase of C rate. The reversible capacity decreases from 1.9 mAh/cm^2 at 0.1 C rate to 1.3 mAh/cm^2 at 1 C rate. Upon returning to cycling at 0.1 C rate, the cell recovers high capacity to 1.9 mAh/cm^2 and keeps good cycling stability in the rest cycles. The cycling stability at lower C rate is apparently better than that at higher C rate.

Figure 12 presents voltage profiles of a full cell using 4-μm-thick Si film as an anode. Except for the first cycle, the cell shows stable cycling performance in the 2nd and 3rd cycles. After the 4th charging, the cell was laid aside on open circuit for 20 days and 25°C in order to examine its self-discharge characteristic. It is found that the potential of the cell decreased by 0.15 V during this period of time and the discharge capacity decreased by 0.1 mAh/cm^2 compared to that in the 3rd cycle. From the 5th cycle, the cell recovers its cycling performance the same as in the 2nd and 3rd cycles. The result indicates that the system has a small self-discharge rate.

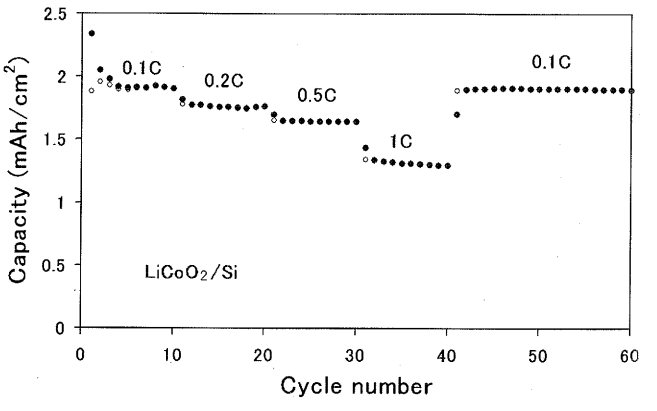

Figure 11. Rate capability of the full cell using the 4-μm-thick Si film as an anode.

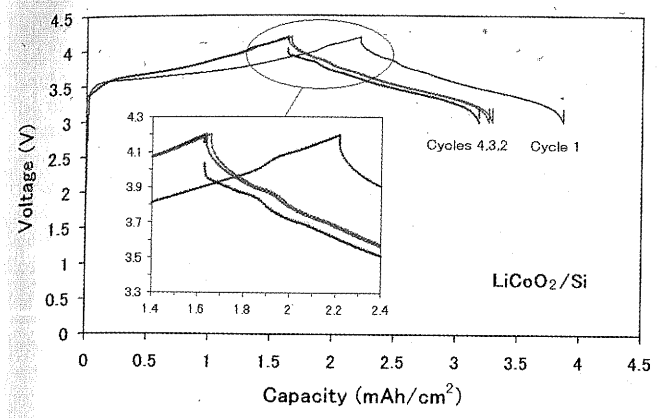

Figure 12. Voltage profiles of the full cell using 4-μm-thick Si film as an anode. After the 4th charging, the cell was laid aside on open circuit for 20 days for examining its self-discharge characteristic.

Conclusions

A series of Si thin films with different thicknesses were fabricated by electron-beam deposition method on the Cu substrate with a specially treated concave-convex surface. The combined analyses involving SEM, TEM, SAED, and XRD revealed that the deposited Si layer possesses good adhesion to the substrate and a discontinuous amorphous microstructure in which there exists large amounts of interface regions. It was considered that this kind of microstructure was beneficial to the electrochemical behaviors of the Si film electrodes.

The half-cell tests demonstrated that these thicker films gave impressive capacity and cycleability; their cycleability could be substantially improved by limiting Li insertion depth. The full-cell tests indicated that the Si films thicker than 4 μm could provide sufficient capacity to match the standard $LiCoO_2$ cathode with an ~70-μm-thick coating layer. Such cells demonstrated small self-discharge rate as well as good cycling stability and efficiency in the long run.

The surface changes of the Si thin-film electrodes during Li insertion and extraction were investigated by GD-OES. The result showed that the unstable SEI layer and the residual lithiated phases are most likely the reason for the irreversible capacity loss.

Acknowledgment

This work was financially supported by the New Energy and Industrial Technology Development Organization (NEDO, Japan, contract no. 51101816).

The National Institute of Advanced Science and Technology assisted in meeting the publication costs of this article.

References

1. J. O. Besenhard, J. Yang, and M. Winter, *J. Power Sources*, **68**, 87 (1997).
2. M. Winter and J. O. Besenhard, *Electrochim. Acta*, **45**, 31 (1999).
3. R. A. Huggins, *Materials for Lithium-Ion Batteries*, C. Julien and Z. Stoynov, Editors, pp. 47-74, Kluwer Academic Publishers, Norwell, MA (2000).
4. O. Mao, R. A. Dunlap, and J. R. Dahn, *J. Electrochem. Soc.*, **146**, 405 (1999).
5. L. Y. Beaulieu and J. R. Dahn, *J. Electrochem. Soc.*, **147**, 3237 (2000).
6. J. Yang, Y. Takeda, N. Imanish, and O. Yamamoto, *J. Electrochem. Soc.*, **146**, 4009 (2000).
7. M. M. Thackeray, J. T. Vaughey, C. S. Johnson, A. J. Kropf, R. Benedek, L. M. L. Fransson, and K. Edstrom, *J. Power Sources*, **113**, 124 (2003).
8. J. Yin, M. Wada, S. Yoshida, K. Ishihara, S. Tanase, and T. Sakai, *J. Electrochem. Soc.*, **150**, A1129 (2003).
9. M. Wada, J. Yin, E. Tanabe, Y. Kitano, S. Tanase, O. Kajita, and T. Sakai, *Electrochemistry (Tokyo, Jpn.)*, **71**, 1064 (2003).
10. J. Yin, M. Wada, S. Tanase, and T. Sakai, *J. Electrochem. Soc.*, **151**, A583 (2004).
11. J. Yin, M. Wada, S. Tanase, and T. Sakai, *J. Electrochem. Soc.*, **151**, A867 (2004).
12. J. Yin, M. Wada, Y. Kitano, S. Tanase, O. Kajita, and T. Sakai, *J. Electrochem. Soc.*, **152**, A1341 (2005).
13. R. A. Huggins, *Solid State Ionics*, **113-115**, 57 (1998).
14. J. Yang, M. Winter, and J. O. Besenhard, *Solid State Ionics*, **90**, 281 (1996).
15. H. Li, X. Huang, L. Chen, Z. Wu, and Y. Liang, *Electrochem. Solid-State Lett.*, **2**, 547 (1999).
16. S. Bourderau, T. Brousse, and D. M. Schleich, *J. Power Sources*, **81-82**, 233 (1999).
17. I. Kim, P. N. Kumta, and G. E. Blomgren, *Electrochem. Solid-State Lett.*, **3**, 493 (2000).
18. S. H. Wang, H. Lee, S. Jang, S. Lee, S. Lee, H. Baik, and J. Lee, *Electrochem. Solid-State Lett.*, **4**, A97 (2001).
19. S.-J. Lee, J.-K. Lee, S.-H. Chung, H.-Y. Lee, S.-M. Lee, and H.-K. Baik, *J. Power Sources*, **97-98**, 191 (2001).
20. L. Y. Beaulieu, K. W. Eberman, R. L. Turner, L. J. Krause, and J. R. Dahn, *Electrochem. Solid-State Lett.*, **4**, A137 (2001).
21. J. Niu and J. Y. Lee, *Electrochem. Solid-State Lett.*, **5**, A107 (2002).
22. S.-W. Song, K. A. Striebel, R. P. Reade, G. A. Roberts, and E. J. Cairns, *J. Electrochem. Soc.*, **150**, A121 (2003).
23. L. Y. Beaulieu, K. C. Hewitt, R. L. Turner, A. Bonakdarpour, A. A. Abdo, L. Christensen, K. W. Eberman, L. J. Krause, and J. R. Dahn, *J. Electrochem. Soc.*, **150**, A149 (2003).
24. P. Limthongkul, Y. Jang, N. J. Dudney, and Y.-M. Chiang, *Acta Mater.*, **51**, 1103 (2003).
25. T. Yoshida, T. Fujihara, H. Fujimoto, R. Ohshita, M. Kamino, and S. Fujitani, *The 11th IMLB*, Monterey, CA, Abstract 48 (2002).
26. I. Yonezu, H. Tarui, S. Yoshimura, S. Fujitani, and T. Nohma, *IMLB 12 Meeting*, Abstract 58, Nara, Japan (2004).
27. T. D. Hatchard and J. R. Dahn, *J. Electrochem. Soc.*, **151**, A838 (2004).
28. J. Graetz, C. C. Ahn, R. Yazami, and B. Fultz, *Electrochem. Solid-State Lett.*, **6**, A194 (2003).
29. J. Graetz, C. C. Ahn, R. Yazami, and B. Fultz, *J. Electrochem. Soc.*, **151**, A698 (2004).
30. J. P. Maranchi, A. F. Hepp, and P. N. Kumta, *Electrochem. Solid-State Lett.*, **6**, A198 (2003).
31. T. Takamura, S. Ohara, M. Uehara, J. Suzuki, and K. Sekine, *J. Power Sources*, **129**, 96 (2004).
32. S. Ohara, J. Suzuki, K. Sekine, and T. Takamura, *J. Power Sources*, **136**, 303 (2004).
33. M. Aramata, M. Uehara, J. Suzuki, K. Sekine, and T. Takamura, in *The 45th Battery Symposium in Japan*, Kyoto, Japan, Nov 27-29, 2004, Abstract 1C04.
34. D. T. Shieh, J. Yin, K. Yamamoto, M. Wada, S. Tanase, and T. Sakai, *J. Electrochem. Soc.*, **153**, A106 (2006).